Van Paepegem, W., Degrieck, J. and De Baets, P. (2001). Finite Element Approach for Modelling Fatigue Damage in Fibre-reinforced Composite Materials. *Composites Part B*, 32(7), 575-588.

Finite Element Approach for Modelling Fatigue Damage in Fibre-reinforced Composite Materials

W. Van Paepegem*, J. Degrieck and P. De Baets

Ghent University, Dept. of Mechanical Construction and Production,
Sint-Pietersnieuwstraat 41, 9000 Gent, Belgium

Abstract

Today, a lot of research is dedicated to the fatigue behaviour of fibre-reinforced composite materials, due to their increasing use in all sorts of applications. These materials have a quite good rating as regards to life time in fatigue, but the same does not apply to the number of cycles to initial damage nor to the evolution of damage. Composite materials are inhomogeneous and anisotropic, and their behaviour is more complicated than that of homogeneous and isotropic materials such as metals. A new finite element approach is proposed in order to deal with two conflicting demands: (i) due to the gradual stiffness degradation of a fibre-reinforced composite material under fatigue, stresses are continuously redistributed across the structure and as a consequence the simulation should follow the complete path of successive damage states; (ii) the finite element simulation should be fast and computationally efficient to meet the economic needs. The authors have adopted a *cycle jump* approach which allows to calculate a set of fatigue loading cycles at deliberately chosen intervals and to account for the effect of the fatigue loading cycles in between in an accurate manner. The finite element simulations are compared against the results of fatigue experiments on plain woven glass/epoxy specimens with a $[\#45°]_8$ stacking sequence.

Keywords: B. Fatigue, C. Finite element analysis, C. Damage mechanics, A. Polymer-matrix composites

Introduction

As a result of their high specific stiffness and strength, fibre-reinforced composites are often selected for weight-critical structural applications. Moreover fibre-reinforced composites have a rather good rating as regards to life time in fatigue, but the same does not apply to the number of cycles to initial damage nor to the evolution of damage. Indeed composite materials are inhomogeneous and anisotropic, and their behaviour is very different from the behaviour exposed by homogeneous and isotropic materials such as metals.
In metals the stage of gradual and invisible deterioration spans nearly the complete life time. No significant reduction of stiffness is observed during the fatigue process. The final stage of the process starts with the formation of one or more small cracks, which is the only form of macroscopically observable damage. Gradual growth and coalescence of these cracks quickly produce a large crack and final failure of the structural component.
Fibre-reinforced plastic composites are made of reinforcing fibres embedded in a polymer matrix. This makes them heterogeneous and anisotropic. The first stage of deterioration by

* Corresponding author (Fax: +32-(0)9-264.35.87, E-mail: Wim.VanPaepegem@rug.ac.be).

fatigue is observable by the formation of more or less extended damage zones, which contain a multitude of microscopic cracks and other forms of damage, such as debonding, initial fracture of fibres,... It is important to notice that damage can start very early, after only a few or a few hundred loading cycles. This early damage is followed by a second stage of gradual deterioration of the material, characterized by a gradual growth of the damage zones and reduction of the stiffness. More serious types of damage appear finally in the third stage, such as fibre breakage and delaminations, leading to an accelerated decline and finally to final failure.

As the stiffness of a metal remains quasi unaffected during fatigue life, the linear relation between stress and strain remains valid, and the fatigue process can be simulated by a linear elastic analysis and linear fracture mechanics in most common cases. Indeed, for metals, often one finite element calculation is done with the assumption of elastic behaviour. Then, in the post-processing stage, the fatigue life of the individual nodes of the finite element mesh is assessed taking into account the (multi-axial) stress state in that particular node. Often the critical plane concept is used for this purpose [1]. In a fibre-reinforced composite, the gradual loss of stiffness in the damaged zones leads to a continuous redistribution of stresses and a reduction of stress concentrations inside a structural component. As a consequence an appraisal of the actual state or a prediction of the final state (when and where final failure is to be expected) requires the simulation of the complete path of successive damage states.

Fatigue models for fibre-reinforced composites can be generally classified in three categories [2]: the fatigue life models which use the information from S-N curves (influence of stress amplitude on occurrence of final failure) or Goodman-type diagrams (influence of mean stress level) and apply some sort of fatigue failure criterion; phenomenological models for residual stiffness/strength; and finally the damage accumulation models developed for specific damage types. Residual stiffness models can be designated for fatigue design of full-scale composite structures, because fatigue life models and residual strength models cannot model the stress redistribution and stiffness reduction. However, the implementation in finite element codes is the prerequisite to bridge the gap between fatigue modelling of laboratory specimens and full-scale components.

This paper presents a new finite element approach, which uses a residual stiffness model to simulate the stiffness reduction and stress redistribution inside a composite component during fatigue life.

Experimental results

In this section a short description of the fatigue experiments, of which the results will be compared against the finite element simulations, is given. A more detailed discussion of the observed experimental results is discussed in other works of the authors [3-4].

Material

The material used in this study was a glass fabric/epoxy composite. The fabric was a Roviglass R420 plain woven glass fabric (Syncoglas) and the epoxy was Araldite LY 556 (Ciba-Geigy). The plain woven glass fabric was stacked in eight layers. The angle between the warp direction of all layers and the loading direction was 45º (denoted as $[\#45^{o}]_8$, where '45°' is the angle between the warp direction of each of the eight layers and the loading direction and where the symbol '#' refers to the fabric reinforcement type). All composite specimens were manufactured using the resin-transfer-moulding technique. After curing they had a thickness of 2.72 mm. The samples were cut to dimensions of 145 mm long by 30 mm

wide on a water-cooled diamond saw and were inspected with optical micrography for presence of any damage.
The in-plane elastic properties of the composite laminates were determined using a micromechanical analysis, where the properties of the E-glass fibre and the epoxy matrix were filled in separately. Since all layers were stacked in the same direction, the elastic properties were valid for both the lamina and the laminate. With the fibre volume fraction V_f being 0.48, the estimated homogenized properties are listed in Table 1. The dimension of the elastic properties is enclosed within square brackets and dimensionless values are indicated with [-]. This convention is used throughout the whole text.

Table 1 Estimated in-plane elastic properties of the $[\#45^o]_8$ composite laminates

E_{11} [GPa]	13.7
E_{22} [GPa]	13.7
ν_{12} [-]	0.525
G_{12} [GPa]	10.5

Experimental setup for bending fatigue

Although fatigue experiments in tension and compression are most often used in fatigue research [5-7], bending fatigue experiments were preferred because they allow to test the finite element implementation in more complicated conditions [8-10]:
- the bending moment is linear along the length of the specimen. Hence stresses, strains and damage distribution vary along the gauge length of the specimen. On the contrary, with tension/compression fatigue experiments, the stresses, strains and damage are assumed to be equal in each cross-section of the specimen,
- due to the continuous stress redistribution, the neutral fibre (as defined in the classic beam theory) is moving in the cross-section because of changing damage distributions. Once that a small area inside the composite material has moved for example from the compressive side to the tensile side, the damage behaviour of that area is altered considerably.

Figure 1 shows the crank-linkage mechanism of the bending fatigue setup.

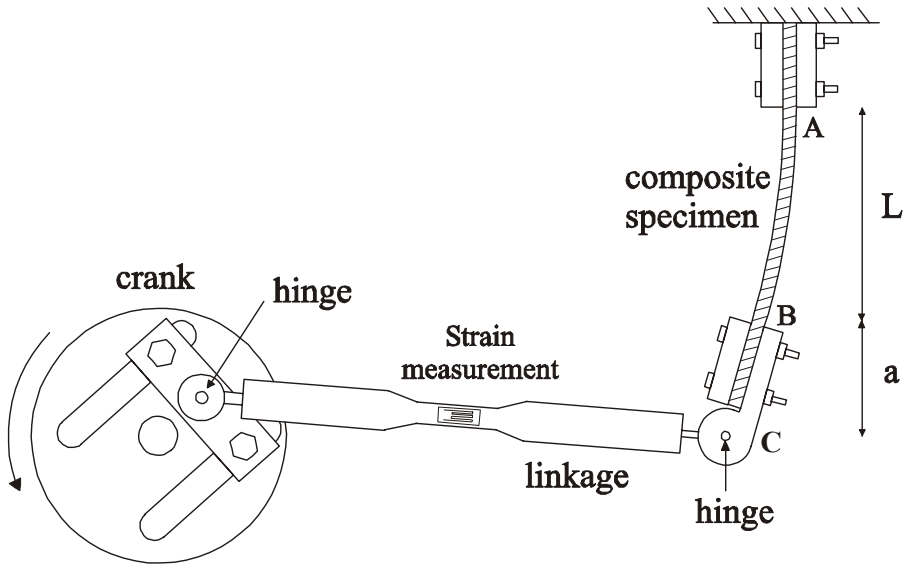

Figure 1 Schematic drawing of the crank-linkage mechanism of the bending fatigue setup [4].

This mechanism imposes an alternating displacement on the hinge (point C) that connects the linkage with the lower clamp of the composite specimen. At the upper end the specimen is clamped. Hence the sample is loaded as a composite cantilever beam. The amplitude of the imposed displacement is a controllable parameter and the adjustable crank allows to choose between single-sided and fully-reversed bending, i.e. the deflection can vary from zero to the maximum deflection in one direction, or in two opposite directions, respectively.
Although neither stresses nor strains are constant along the length of the specimen (only a constant displacement is imposed at the lower end of the specimen), the geometry and loading conditions are very simple, so that the modelling of the experimental layout is still relatively straightforward.

Experimental results

Fatigue experiments were performed with different values of the imposed displacement, as well as with single-sided and fully-reversed bending [4]. To characterize each experiment, the 'displacement ratio' $R_d = \frac{u_{min}}{u_{max}}$ (analogous to the stress ratio R) is defined, whereby the minimum deflection is not necessarily zero. When the displacement u_{max} and the length L between the both clamps (Figure 1) are further given too, the parameters of the fatigue experiment are known.
Figure 2 shows a typical force-cycle history for the $[\#45^o]_8$ specimens. The abscissa contains the number of cycles; the ordinate axis shows the force (Newton), which is measured by a strain gauge bridge (Figure 1) during the fatigue tests at constant bending displacement.

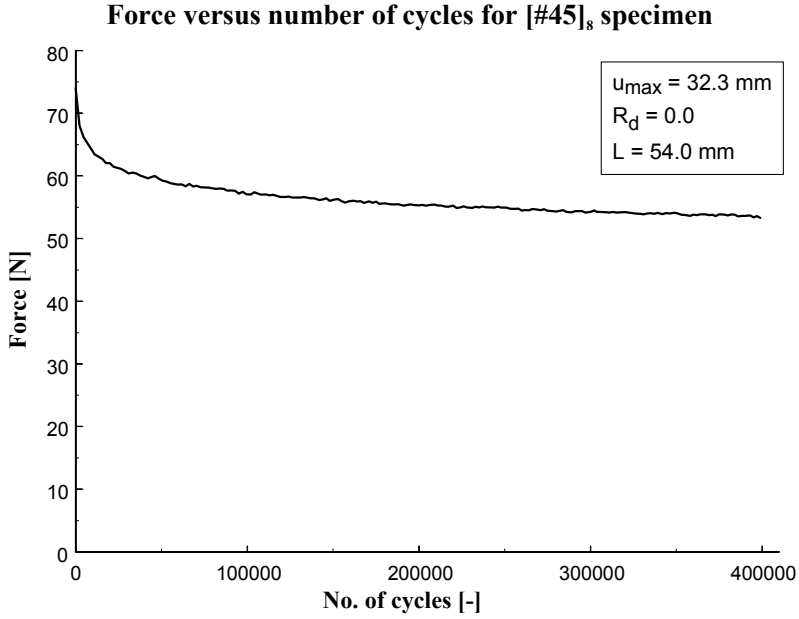

Figure 2 Typical force-cycle history for a plain woven glass/epoxy specimen with $[\#45^o]_8$ stacking sequence.

In this typical experiment the specimen is fatigued in single-sided bending while the imposed displacement varies between zero (R_d = 0.0) and u_{max}. The gradual stiffness reduction, as shown on the graph, will now be modelled by a local damage model in the next paragraph.

Local damage model

The finite element approach outlined further must of course not be limited to the fatigue modelling of the glass/epoxy composite material used in this study. The dependence on the studied material is expressed only by the choice of the fatigue model which describes the behaviour under fatigue of this material. For other materials another fatigue law will eventually have to be implemented. In this study the capability of several fatigue models to describe the fatigue damage behaviour of the glass fibre-reinforced composite material was investigated. A fatigue damage model, very similar to the one proposed by Sidoroff and Subagio [11], was adopted here to demonstrate the finite element approach. It is given by:

$$\frac{dD}{dN} = \begin{cases} \dfrac{A \cdot \left(\dfrac{\Delta\sigma}{\sigma_{TS}} \right)^c}{(1-D)^b} & \text{in tension} \\ 0 & \text{in compression} \end{cases} \qquad (1)$$

where:
- D : local damage variable
- N : number of cycles
- $\Delta\sigma$: amplitude of the applied cyclic loading
- σ_{TS} : initial static tensile strength
- A, b and c : three material constants

The local damage variable D is associated with the longitudinal stiffness loss. Hence the fatigue damage law applies to uniaxial loading conditions and the damage value is lying between *zero* (virgin state of the material) and *one* (complete failure of the material). The stresses and strains are related by the commonly used equation in damage mechanics: $\sigma = E_0.(1-D).\varepsilon$. The assumption in the fatigue damage law (Equation (1)) that damage is not growing in the regions subjected to compressive stresses, is justified because in the experiments no micro-buckling or any macroscopically significant damage could be observed at the surface that was subjected to compressive stresses.

Semi-analytical implementation

First a semi-analytical implementation of the fatigue damage model will be discussed, because some important choices of the finite element approach are based on the experiences with this simplified semi-analytical implementation. A detailed discussion of this semi-analytical implementation can be found in [4]. Here only the relevant equations are summarized.

The constitutive equations for stresses and strains are based on the classical beam theory. Figure 3 illustrates the corresponding beam model for Figure 1 and the bending moment distribution along the specimen length. The composite specimen is considered as a bending cantilever beam, connected with a rigid rod (the lower clamp of the linkage). At the end of

that rigid rod, the harmonic displacement u(C) is imposed. The force F is the necessary force to impose this bending displacement u(C).

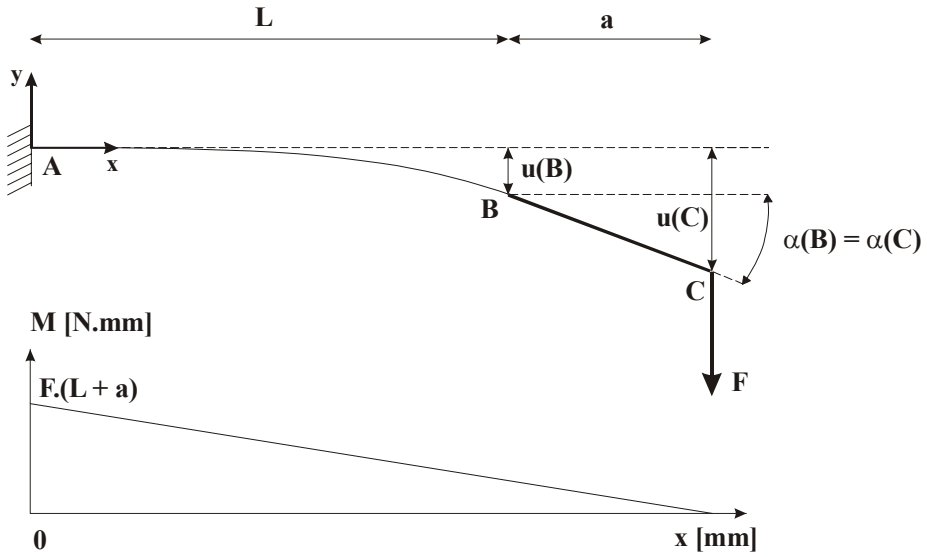

Figure 3 Classical beam theory applied to the cantilever composite specimen.

The stresses and strains are calculated from the well-known equations:

$$\varepsilon_{xx}(x,y) = \frac{-M(x)\left(y - y_0(x)\right)}{EI(x)}$$
$$\sigma_{xx}(x,y) = E_0\left(1 - D(x,y)\right)\varepsilon_{xx}(x,y) \qquad (2)$$

where M(x) is the bending moment distribution along the specimen length, $y_0(x)$ is the position of the neutral fibre and EI(x) is the global bending stiffness EI of each cross-section along the specimen length. The damage growth rate dD/dN is described by the residual stiffness model in Equation (1).
It is very important to take into account in Equation (2) a possible shift of the neutral fibre $y_0(x)$. When the axial force is supposed to remain zero and when only a bending moment exists, the position of the neutral fibre $y_0(x)$ at each moment of time is calculated as:

$$y_0(x) = \frac{\int_{-\frac{h}{2}}^{+\frac{h}{2}} \left[1 - D(x,y)\right].y \, dy}{\int_{-\frac{h}{2}}^{+\frac{h}{2}} 1 - D(x,y) \, dy} \qquad (3)$$

where : - y : thickness-coordinate, with y = 0 in the middle of the specimen thickness
- h : total thickness of the specimen

The degraded bending stiffness EI(x) becomes (with 'b' the specimen width):

$$EI(x) = b.E_0.\int_{-\frac{h}{2}}^{+\frac{h}{2}} \left[1 - D(x,y)\right].y^2 \, dy \tag{4}$$

Since the bending fatigue experiments are displacement-controlled, the corresponding force F, necessary to impose the bending displacement, must be determined. Using the virtual work principle for a cantilever beam loaded in point B with a vertical force F and a bending moment F·a, the expressions are:

$$\begin{aligned} u(B) &= F\cdot\int_0^L \frac{(L-x)^2}{EI(x)}dx + F\cdot a\cdot\int_0^L \frac{(L-x)}{EI(x)}dx \\ \alpha(B) &= F\cdot\int_0^L \frac{(L-x)}{EI(x)}dx \; + F\cdot a\cdot\int_0^L \frac{1}{EI(x)}dx \end{aligned} \tag{5}$$

where : - F : force measured by the strain gauges and acting on the hinge (point C in Figure 1),
- a : length of the lower clamp (Figure 1).

The unknown force F is then solved from the resulting transcendental equation:

$$u(C) = u_{max} = u(B) + a.\sin\left(\alpha(B)\right) \tag{6}$$

The parameter u_{max} is the same as the one that appears in the definition of the displacement ratio R_d.

This analytical model can be easily implemented in a mathematical software package such as Mathcad™. The numerical integration formulae must be chosen such that the second degree polynomials are exactly integrated. This is the case for the Simpson's rule, which is a Newton-Cotes quadrature formula. Because the increase of the damage variable D during one cycle is so small, the integrations must be exact indeed, otherwise the relative error on the calculation of the bending stiffness EI(x) may be larger than the increase of the damage variable itself. Therefore the conventional first-order trapezium method is not suited for this purpose.

First the distribution of the bending moment along the length of the specimen is determined. Secondly the stresses and strains in each integration point of the mesh are calculated. The damage law is applied and a new cycle is evaluated. From Equation (6) the necessary force to impose the displacement with amplitude u_{max} can be calculated for each cycle.

Yet the remaining problem is that the numerical implementation deals with two important, but contradictory demands:

- in order to correctly predict the damage and residual stiffness of the composite structure after a certain number of cycles, the simulation should trace the complete path of successive damage states to keep track of the continuous stress redistribution,
- the numerical simulations should be fast and computationally efficient. It is impossible to simulate each of the hundreds of thousands of loading cycles for a real construction, or even for a part of it. Indeed, even for this simplified Mathcad™ implementation, the computational effort to simulate each of half a million loading cycles is huge. Moreover

several parameters must be saved for each loading cycle, so that arrays with a length of half a million records must be stored in memory.

It is evident that only a selected set of loading cycles can be simulated, but how should this set be determined ? This key question will now be investigated for the semi-analytical implementation, but the conclusions will be applied to the finite element implementation, where the limitation of the computational effort is even more stringent.

To make the reader familiar with the kind of obtained results, a simulation is done with a *fixed* array of cycle numbers at which the fatigue damage law will be evaluated. The interval between two successive cycle numbers is very small at the first few cycles and is then increasing further on (N = 1, 2, 3, 8, 18, 37, 65, 138,…). The imposed displacement u_{max} was chosen to be 32.3 mm and the calculation was stopped at 400,000 cycles to comply with the experimental results from Figure 2. The simple Euler explicit integration formula was used to evaluate the local increase of damage for each integration point over each interval NJUMP = N_{i+1} - N_i :

$$D_{N+NJUMP} = D_N + \left.\frac{dD}{dN}\right|_N \cdot NJUMP \tag{7}$$

The flowchart of this numerical Mathcad^{TM} simulation (with a *fixed* set of simulated loading cycles) is shown in Figure 4.

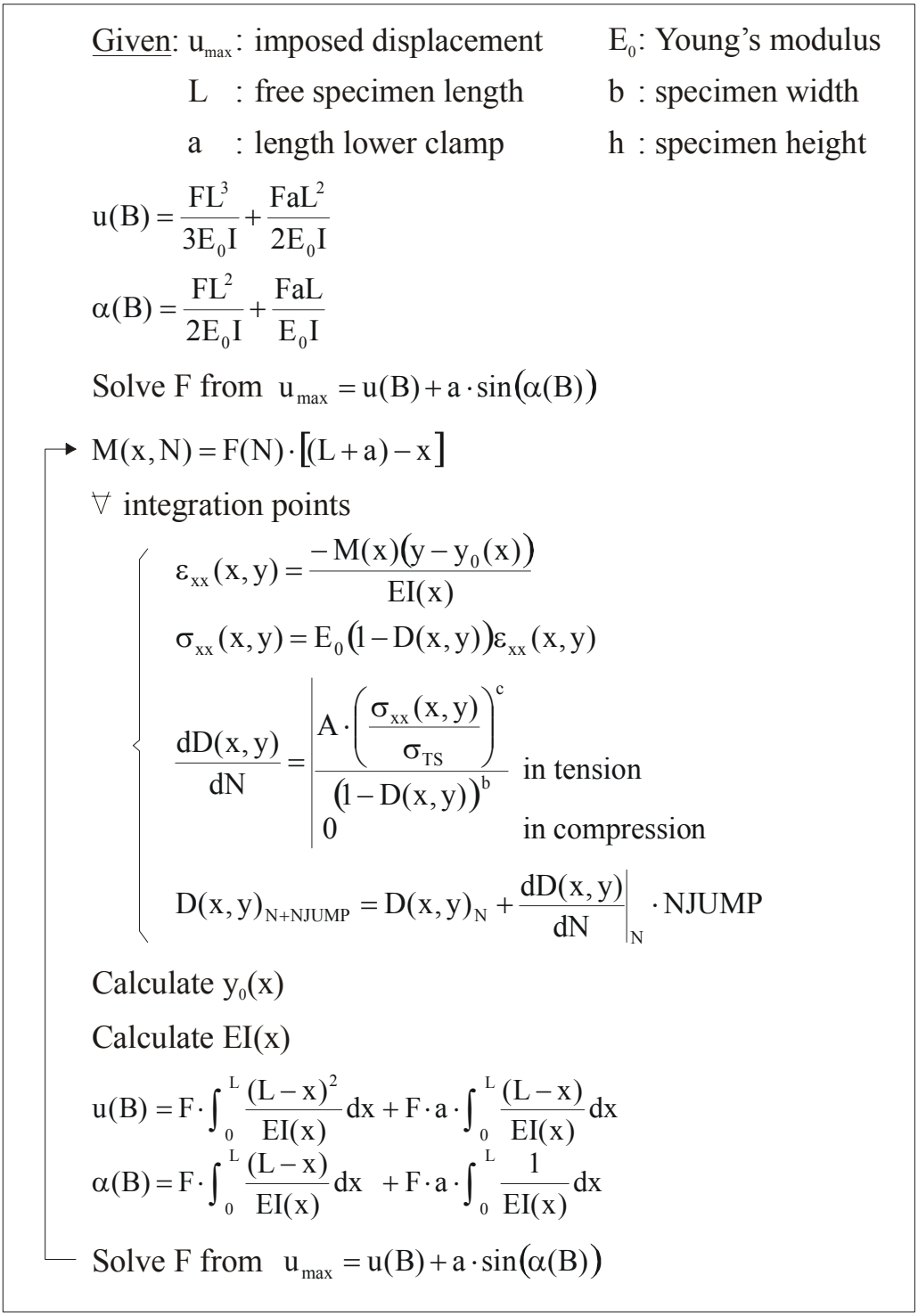

Figure 4 Flow-chart of the Mathcad™ implementation with fixed *cycle jumps*.

Figure 5 shows the resulting force-cycle history for a well-chosen set of the constants A, b and c (see Equation (1)), being respectively $9.4 \cdot 10^{-4}$ [1/cycle], 0.45 [-] and 6.5 [-]. The initial static tensile strength σ_{TS} was 201.2 [MPa].

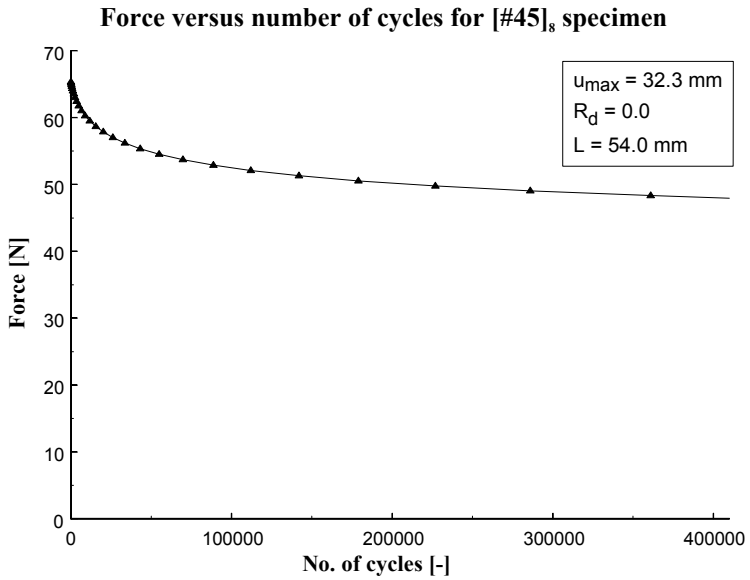

Figure 5 Simulated force-cycle history with a fixed array of cycle numbers.

It is worthwile to note that there is already a close agreement with the experimental results shown in Figure 2. Now the simulated results at some interesting integration points of the mesh will be investigated. In Figure 6 a detail of the mesh is shown. The integration points of interest are chosen at the clamped cross-section x = 0, and their position is marked with a dot (y = -0.272 mm, 0.0 mm, 0.544 mm and 1.36 mm). Positive y-values correspond with integration points at the tension side and negative y-values with integration points at the compression side. As was mentioned earlier, the full thickness of the composite specimens was 2.72 mm and the origin of the y-axis is in the midplane of the laminate.

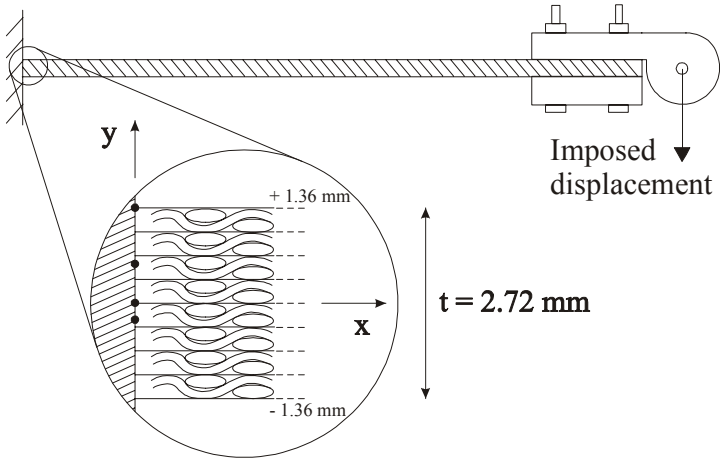

Figure 6 Position of the integration points of interest: x = 0 mm, and y = -0.272 mm, 0.0 mm, 0.544 mm and 1.36 mm.

In the Figures 7 – 10, the stress-cycle histories are now plotted for these four integration points at the clamped cross-section.

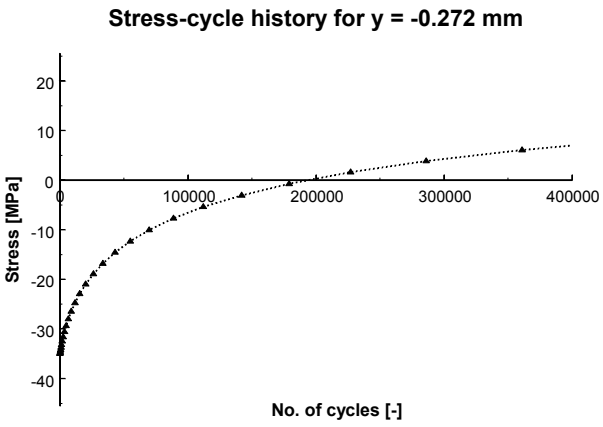

Figure 7 Stress-cycle history for y = -0.272 mm

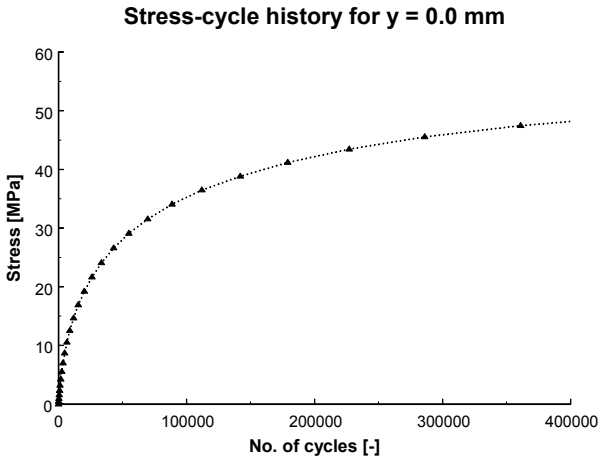

Figure 8 Stress-cycle history for y = 0.0 mm

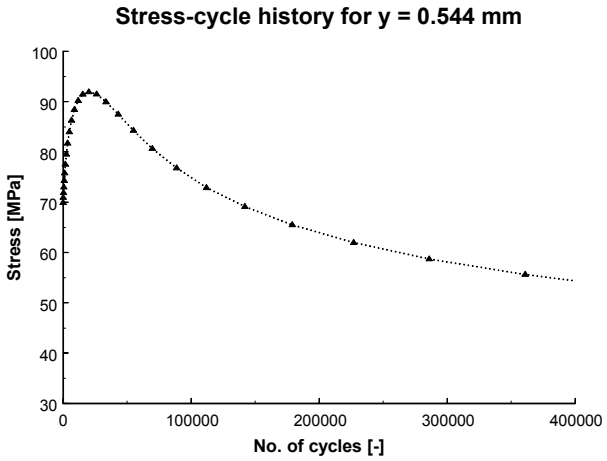

Figure 9 Stress-cycle history for y = 0.544 mm

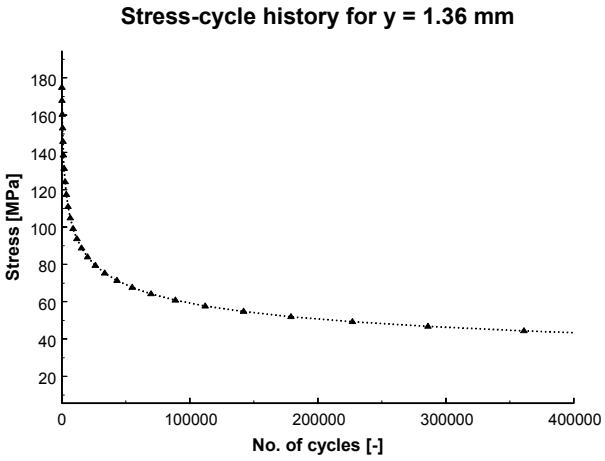

Figure 10 Stress-cycle history for y = 1.36 mm

It is very important to note that these stress-cycle curves are not at all some sort of master curves or S-N curves to predict the behaviour of a certain integration point at a certain stress level. At each simulated cycle, these stresses result from the equilibrium stress state of the composite specimen for the applied imposed displacement and the stiffness distribution which is governed by the residual stiffness model (Equation (1)). As indicated at the flow-chart in Figure 4, the change of the stress state in each integration point during fatigue life is governed exclusively by the stiffness degradation $E(x,y)/E_0$ which can vary from point to point, because the stress amplitude $\sigma_{xx}(x,y)$ in the expression $dD(x,y)/dN$ might be different for each Gauss point considered.

From the Figures 7 – 10, it appears that the shape of the stress-cycle curves can be very different:

- the integration point y = - 0.272 mm initially lies at the compression side, but due to the stress redistribution at the clamped cross-section, the normal stress is changing from compressive stress (-) to tensile stress (+),
- the integration point y = 0.0 mm is the neutral fibre of the virgin state material, but due to the stress redistribution, the stress is becoming increasingly positive,
- the integration point y = 0.544 mm is lying at the tension side, and due to the load transfer from the heavily damaged neighbouring zone, the tensile stress is first increasing but going downhill afterwards,
- the integration point y = 1.36 mm is lying at the specimen surface at the tensile side and the stress-cycle curve is showing a very sharp decline, because the high initial value of the stress amplitude σ_{xx} leads to a large damage growth rate dD/dN in the first few cycles.

The information about the stress state of all integration points at the clamped cross-section can now be combined in Figure 11 where the distribution of normal stress at the clamped cross-section of the composite specimen is plotted for increasing numbers of loading cycles. The abscissa contains the value of the normal stress, while the ordinate axis represents the total thickness of the specimen ($y \in [-1.36\text{ mm}, +1.36\text{ mm}]$)

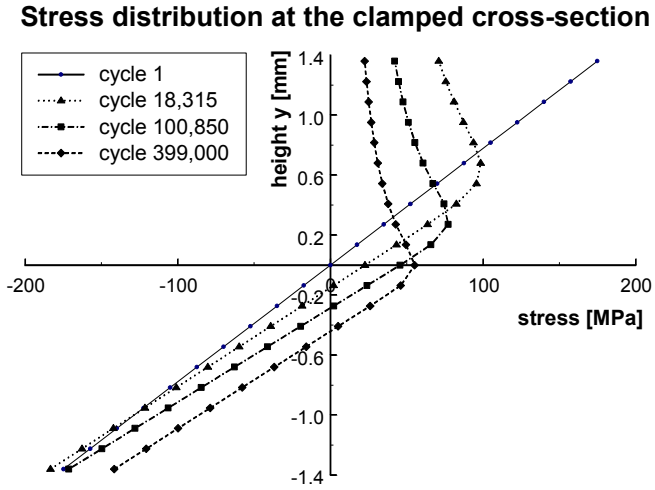

Figure 11 Normal stress distribution at the clamped cross-section of the $[\#45^o]_8$ specimen, calculated with the semi-analytical Mathcad™ approach [4].

At the first cycle, the stress distribution is symmetric with respect to the midplane and the normal stress is zero in the middle of the cross-section. Since the equations of classical beam theory were used to calculate bending moments and strains, this result was to be expected. When damage is initiating, the tensile stresses in the outermost layers are relaxed and load is transferred towards the inner layers. Because the damage law assumes that there is no damage growth at the compressive side, the peak tensile stresses are moving towards the compression side and the neutral fibre is moving down. Thus, as stated earlier, the gradual deterioration of a fibre-reinforced composite – with a loss of stiffness in the damaged zones – leads to a continuous redistribution of stresses and strains, and a reduction of stress concentrations inside a structural component.
In the Figures 12 – 15, the corresponding damage-cycle histories are plotted for the same four integration points (y = -0.272 mm, 0.0 mm, 0.544 mm and 1.36 mm). The damage value is lying between zero and one, while the value for the cycle number N ranges from 1 to 400,000

cycles. The scale of the ordinate axis has been adjusted for each figure, because the different damage values differ several orders in magnitude.

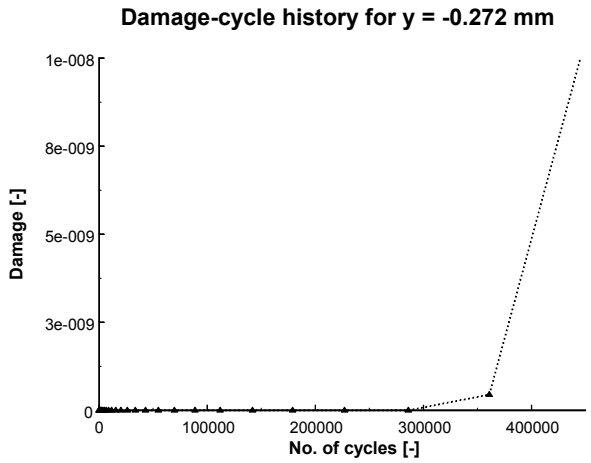

Figure 12 Damage-cycle history for y = -0.272 mm

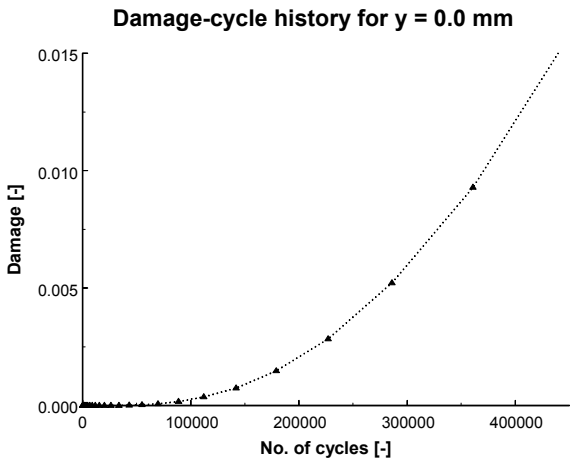

Figure 13 Damage-cycle history for y = 0.0 mm

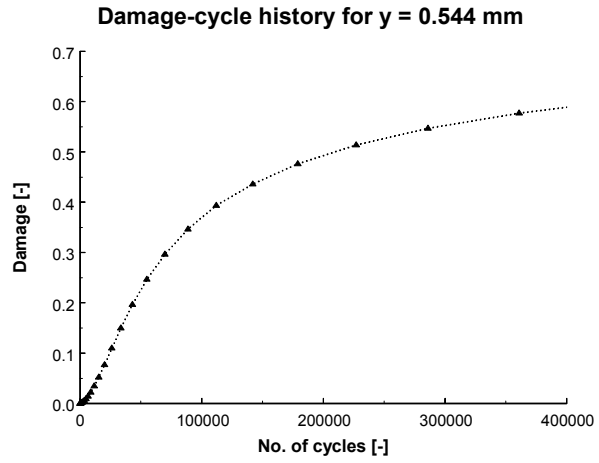

Figure 14 Damage-cycle history for y = 0.544 mm

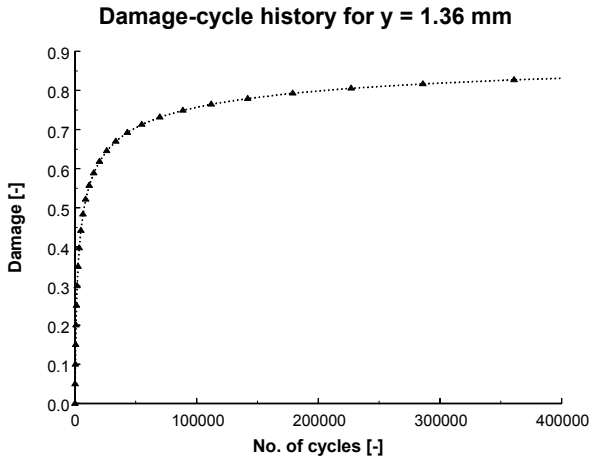

Figure 15 Damage-cycle history for y = 1.36 mm

For all simulated results so far, a *fixed* set of simulated loading cycles was used. However, for more complex geometries and/or fatigue loadings, it is difficult to assess when the *cycle jumps* can be taken larger without jeopardizing the accuracy, and when very small *cycle jumps* are necessary to adequately simulate the stress redistribution. Therefore an automatic algorithm should be developed to determine the size of the *cycle jumps* during the simulation of the whole fatigue life.

To automate the choice of this set of cycle numbers where the damage growth law is evaluated for each integration point, a criterion could be imposed to the stress components, to the damage variable(s) or to some weighted combination of them. It appears now that the damage curves have some favourable properties as compared to the stress curves. Indeed,

although the damage curves of the integration points can be rather different in shape, they have two important advantages for extrapolation, compared to the stress curves:
- the value of the damage variable D is always lying between known values; *zero* (virgin state material) and *one* (complete failure of the material),
- the gradient dD/dN has to be positive or zero. The curve can never decrease, because the damage state reached cannot be reversed anymore. On the other hand, depending on load redistributions, stresses can increase or decrease, without any foreknowledge.

These properties of the damage curves remain when considering complex stress-cycle histories of real in-service fatigue loadings. In such multi-axial loading conditions, several stress components will affect the material's fatigue behaviour, while each of them can decrease or increase at different moments in fatigue life. Extrapolating these stress-cycle histories is a hazardous job, because it is almost impossible to define a common procedure that can cope with the extrapolation of such dissimilar stress-cycle histories.
Therefore, the automatic calculation of the *cycle jumps* NJUMP will be based on a criterion for the damage curves. The idea of the corresponding *cycle jump* approach is shown in Figure 16: the computation is done for a certain set of loading cycles at deliberately chosen intervals, and the effect on the stiffness degradation of these loading cycles is extrapolated over the corresponding intervals in an appropriate manner. The cycles in continuous line are simulated in physical time, while the *cycle jumps* are performed at the time scale of the number of loading cycles.

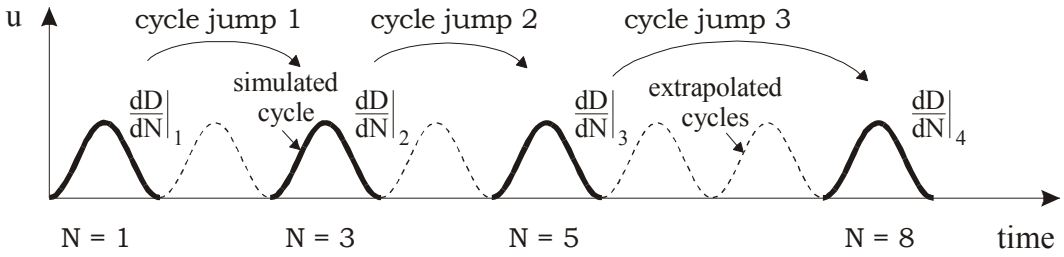

Figure 16 Illustration of the *cycle jump* principle.

The only difference with the Mathcad™ simulations above, is that the value of the *cycle jumps* NJUMP should not be *fixed* in advance, but will be determined by an automatic criterion. In the following paragraph, the finite element implementation will now be discussed. The damage curves of the integration points will be used to extract a criterion to determine the set of simulated loading cycles.

Finite element implementation

The above-mentioned semi-analytical implementation in Mathcad™ has several drawbacks:
- although non-linear material behaviour is accounted for through the introduction of a damage variable D, geometrical non-linearities are not taken into account. However, they should be, because the deformations are so large that geometrical non-linearity does affect the results. This has been proved by linear and non-linear geometric static analyses with finite elements,

- a more complicated geometry of the component is difficult to handle, because only few closed-form solutions do exist to calculate stresses and strains in structures with a complicated cross-section,
- when the structure is subjected to fatigue loadings in multi-axial conditions, the classical beam theory does not suffice to solve the problem,
- preprocessing and postprocessing facilities are very limited.

As a consequence it seems obvious to make use of finite elements to counteract these restrictions.

Since each fatigue loading cycle represents a physical amount of time (frequency = number of cycles per second), the size of the *cycle jump* NJUMP must be the same for all simulated parts of the structure under fatigue, otherwise the next simulated loading cycle N+NJUMP would not be the same for all simulated parts of the composite structure. It is obvious that the calculation of the equilibrium stress state of the fully simulated composite structure makes no sense if the *cycle jump* for one part of the structure is different from the *cycle jump* for another part. However the restrictions on the size of the *cycle jump* can be very contradictory for different parts of the structure:

- the stress distribution in parts of the structure which are loaded with a very low stress level, will remain nearly unchanged and it would be rather safe to jump over a large number of cycles without leading to erroneous estimates of the damage distribution and growth in this domain of the structure,
- other parts of the structure are loaded with high stress levels and damage is growing fast through the successive loading cycles. Then stress is redistributing continuously and load is transferred to neighbouring zones due to the inability of the completely damaged zone to sustain the load furthermore. The *cycle jump* for such parts should be small, otherwise the redistribution of stresses will be modelled inaccurately.

This, together with the idea that finite element meshes are inherently discrete in nature and that (material) properties are attached to discrete integration points of the structure (i.e. the Gauss-points of the mesh), legitimate the assumption that an estimated size of the *cycle jump* could be assigned to each Gauss-point as one of its inherent properties. Of course, as has been mentioned earlier, there can be no more than one global value of the *cycle jump*, since the *cycle jump* is in fact a jump over a certain amount of physical time (number of cycles N, divided by the frequency f). This amount of time has to be the same for all Gauss-points and thus for the whole structure.

In the following paragraphs, we will explain first how a reasonable estimate of the size of the local *cycle jump* for each Gauss-point can be made. Next the global *cycle jump* for the overall structure will be calculated from these values.

Determination of the local cycle jump NJUMP1

The implementation in a finite element code requires the creation of an additional state variable assigned to each Gauss-point of the structure. Beside the damage variable D, this second state variable is the size of the local *cycle jump*, which will be referred to as NJUMP1, an integer value lying between *one* (*cycle jump* over one cycle) and a certain upper limit, which is the maximum number of cycles that can be jumped over, so that the extrapolation of the damage state of that particular Gauss-point toward the loading cycle N+NJUMP1 is within acceptable limits of accuracy.

From the discussion about the semi-analytical implementation, it has been shown that the damage curves have some important advantages compared against the stress curves. Therefore the damage value has been chosen to determine the local *cycle jumps* and it is

matter now of defining the criterion for calculating the NJUMP1 values. The clue to define the value of the local *cycle jump* NJUMP1, is to impose an allowed increase of the damage variable D, which is still considered to be accurate and beyond which limit the value of D may be extrapolated less accurately. One possible and straightforward method is to use the simple Euler explicit integration formula for evaluating the local increase of damage for each Gauss-point:

$$D_{N+NJUMP1} = D_N + \left.\frac{dD}{dN}\right|_N \cdot NJUMP1 \tag{8}$$

The value of the local *cycle jump* NJUMP1 can then be determined by imposing a maximum allowed increase to the damage variable D. For example, $D_{N+NJUMP1}$ can be limited to D_N + 0.01, when the D-values are in the range [0,1[. When the increase dD/dN is limited to for example 0.01, this is equivalent to a piecewise integration of the damage evolution law for that integration point with a step-size of 0.01 along the ordinate axis of the damage-cycle history. This assures an accurate follow-up of the damage path for that integration point. For certain integration points NJUMP1 will be very small, while for Gauss-points lying in low stress zones, it will be very large.
The followed approach can best be illustrated with a simple numerical example. The curve D(N) for a certain Gauss-point is plotted in Figure 17, the values for A, b, c and σ_{TS} being respectively $9.4 \cdot 10^{-4}$ [1/cycle], 0.45 [-], 6.5 [-] and 201.2 [MPa]. The value of the damage variable D at cycle N=60,800 – which has been fully simulated – is 0.60.

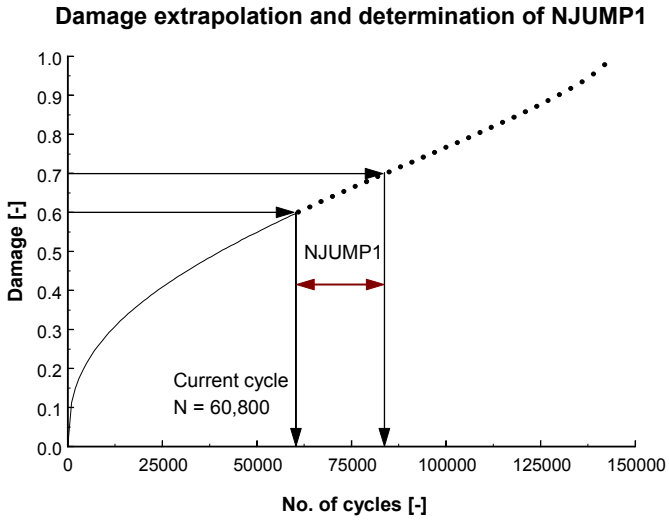

Figure 17 Numerical example of the calculation of the local *cycle jump* NJUMP1.

The damage growth rate dD/dN for this particular Gauss-point at this cycle equals $4.32 \cdot 10^{-6}$ [1/cycle] for D = 0.6 [-] and $\Delta\sigma$(N=60,000) = 82.5 [MPa] (Equation (1)). In this example the increase is limited to an increment of 0.1. The allowed *cycle jump* NJUMP1 then is:

$$\mathrm{NJUMP1} = \frac{(\mathrm{D_N} + 0.1) - \mathrm{D_N}}{\left.\frac{\mathrm{dD}}{\mathrm{dN}}\right|_{\mathrm{N}}} = \frac{0.1}{4.32 \cdot 10^{-6}} = 23{,}143 \text{ cycles} \tag{9}$$

Based on the same philosophy, more accurate numerical techniques can be applied. For example, the damage D could be numerically extrapolated to D + 0.1, taking into account the full damage-cycle history information, instead of using only the last known damage value with the Euler method. However this does not limit the applicability of the approach presented here.

Determination of the global cycle jump NJUMP

Now that the local *cycle jump* NJUMP1 is determined for each Gauss-point, there has to be defined a global *cycle jump* NJUMP, which will be the definitive *cycle jump* for the whole composite structure.
The simplest approach is to define NJUMP as the minimum value of all NJUMP1 values, but this is not recommended, because normally at each moment in the fatigue life of the composite structure, there are Gauss-points with a fast increasing damage variable D; hence the NJUMP1 value will be small. As a consequence, the global *cycle jump* NJUMP will always be small and the calculation will proceed too slowly.
Therefore, the global *cycle jump* NJUMP is defined in another way. First the frequency distribution of all NJUMP1 values is determined. Suppose that the maximum allowed value of the *cycle jump* is 100,000 cycles. To determine the frequency distribution, the range of 100,000 cycles is divided into a number of intervals, called 'classes' in the statistics terminology. Then it is counted how many NJUMP1 values are lying in a particular class. This number, divided by the total number of NJUMP1 values, is the relative frequency of that particular class.
Figure 18 shows an example of such a frequency distribution for the finite element calculation of a standard bending fatigue experiment. There are 838 Gauss-points and the number of classes of the frequency distribution is 100; the length of each of the classes is 1,000 cycles. It is worthwhile to note that there are a small number of Gauss-points in the class [93,000;94,000[cycles. For these Gauss-points a very large *cycle jump* seems safe, although for the vast majority of the Gauss-points the *cycle jump* stays below 20,000 cycles.

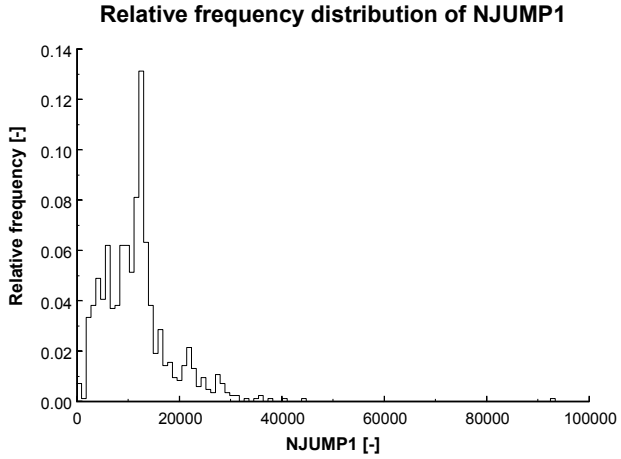

Figure 18 Frequency distribution of NJUMP1

Figure 19 then shows the cumulative relative frequency distribution, where the relative frequencies from Figure 18 are accumulated for increasing class number. NJUMP can best be taken as a small percentile of the cumulative relative frequency distribution of all NJUMP1 values. A little percentage of the Gauss-points will then be imposed a larger *cycle jump* than the NJUMP1 value that was considered to be safe for these Gauss-points. However these Gauss-points will just be the ones that are already seriously damaged and where extrapolation errors will be rather negligible. When for example the 10 % percentile is considered, the value of the global *cycle jump* NJUMP would be 4078 cycles for the example in Figure 19.

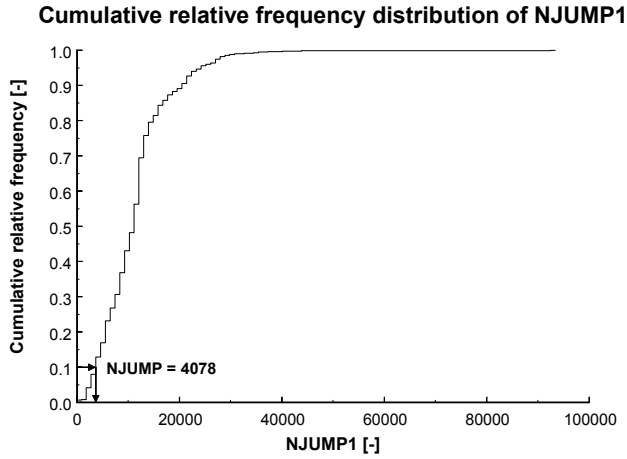

Figure 19 Cumulative frequency distribution of NJUMP1

Finally, Figure 20 shows a detailed flow-chart of the finite element implementation of the *cycle jump* approach. As was mentioned for the semi-analytical implementation, the resulting stress-cycle histories in each Gauss-point are not at all predetermined or empirical in nature. They result from the equilibrium stress state in the composite specimen for the given fatigue loading and stiffness distribution. The stiffness degradation and its distribution is changing during fatigue life in accordance with the residual stiffness model in Equation (1). Through the successive *cycle jumps*, the damage evolution law dD/dN is integrated piecewise for each Gauss-point with $\Delta\sigma$ being the stress amplitude in that particular Gauss-point.
The implementation of the *cycle jump* approach has been done in the commercial finite element code SAMCEF^{TM}. In the next paragraph the results of the finite element calculations will be discussed.

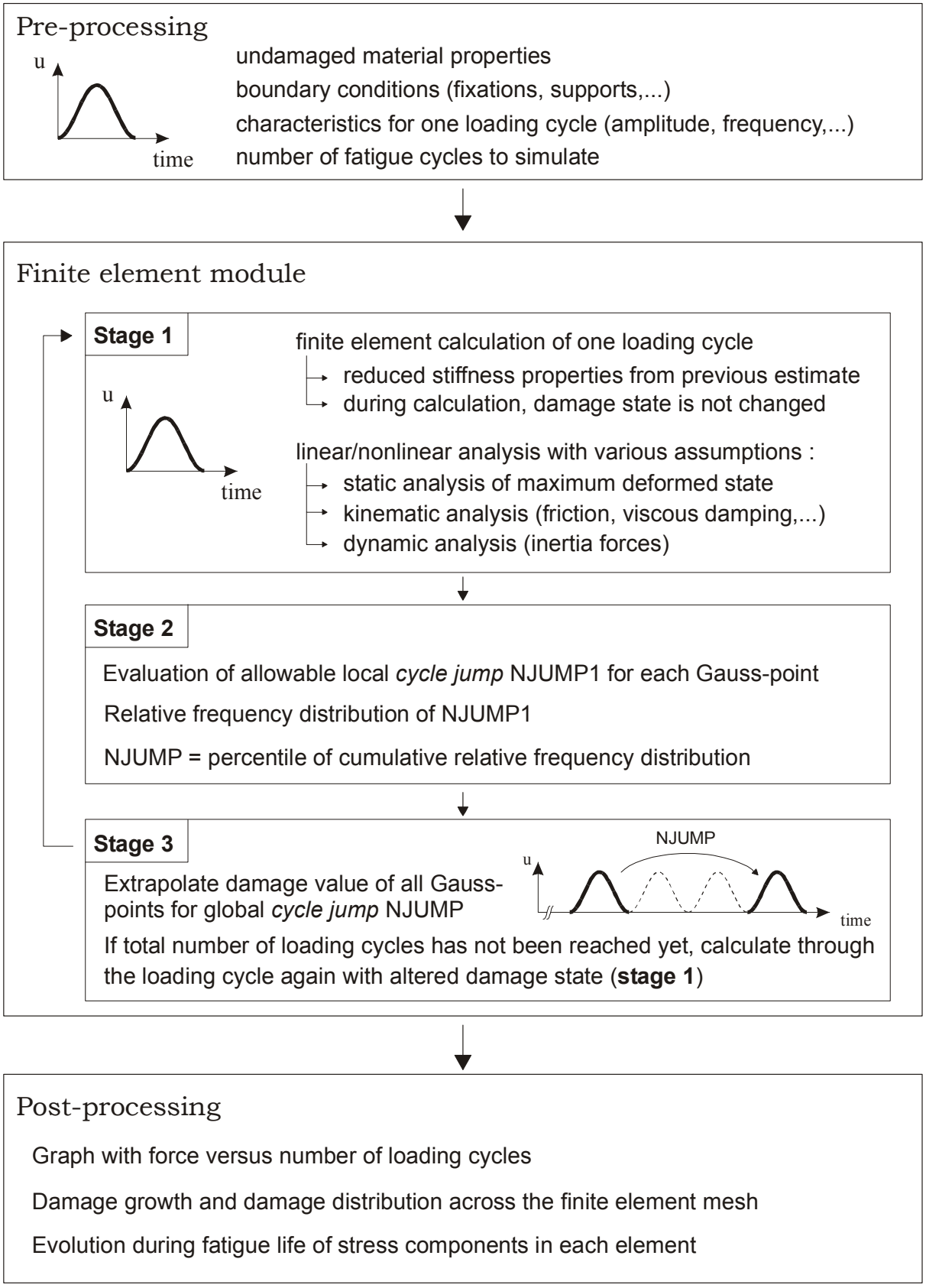

Figure 20 Flow-chart of the finite element implementation of the *cycle jump* approach.

Discussion of results

FEM-model

The finite element model used to simulate the fatigue test of Figure 1 consists of eight layers of composite elements. There are 8 elements through the thickness of the composite specimen and there are 53 elements along the length of the specimen. The lower clamp of the bending fatigue setup (Figure 1) is modelled as a rigid body element and the upper clamp is modelled to be completely fixed. A schematic drawing of the finite element mesh is shown in Figure 21, together with a detail of the finite element mesh where each Gauss-point has been assigned two state variables: the damage value D and the local *cycle jump* NJUMP1.

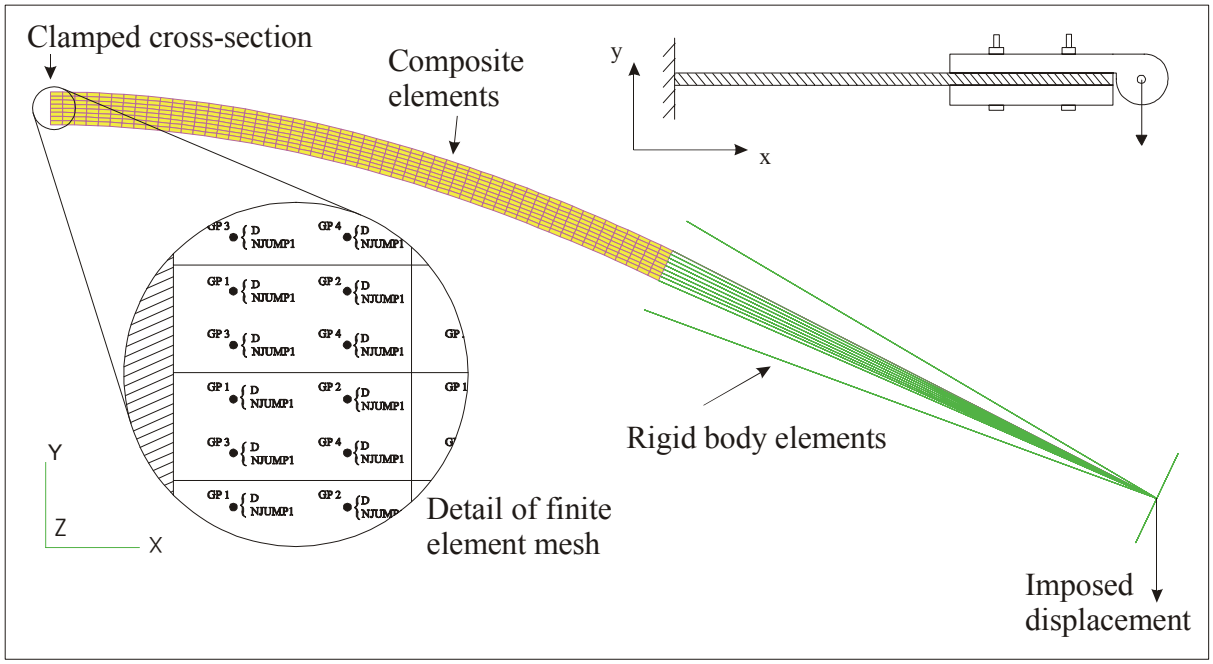

Figure 21 Finite element model of the bending fatigue experiments.

The calculations have been done with the commercial finite element code SAMCEF™ on a SUN Ultra 30 Creator Workstation with a 300 MHz processor and 240 MB RAM. For a simulation of about 400,000 cycles, the calculations last approximately four hours.

Simulations

The parameters A, b and c in the Equation (1) were optimized with a non-linear optimization procedure. The starting values for the parameters were those obtained from the semi-analytical calculation, i.e. $9.4 \cdot 10^{-4}$ [1/cycle], 0.45 [-] and 6.5 [-] respectively. Since the calculated stress states are somewhat different for the finite element simulation and the semi-analytical calculation (due to the simplified assumptions of the classical beam theory), the value of the constants was slightly different and the optimized values for the finite element simulation of the standard bending fatigue experiment were: $9.8 \cdot 10^{-4}$ [1/cycle], 0.42 [-] and 6.53 [-].
Figure 22 shows the comparison between the experimentally measured and the numerically simulated force-cycle history.

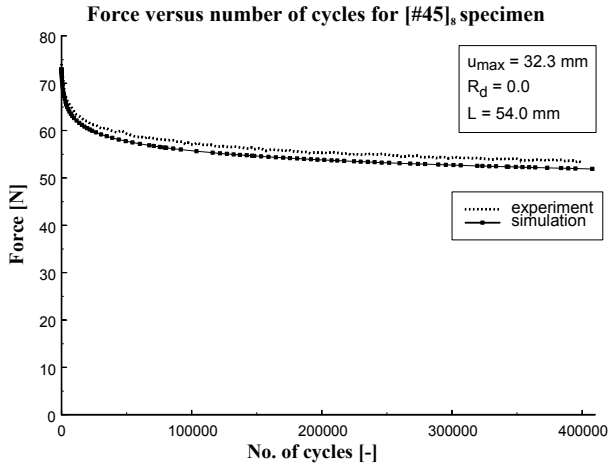

Figure 22 Experimental results versus finite element simulation for a $[\#45^o]_8$ composite specimen.

For the finite element simulation of about 400,000 cycles, 107 *cycle jumps* were taken. The global *cycle jump* NJUMP was defined as the 10% percentile of the cumulative relative frequency distribution of the NJUMP1 values. The reaction force in the node where the displacement u_{max} was imposed (Figure 21), equals 51.9 N at cycle N = 407,898. The experimentally measured force at cycle N = 399,000 was 53.3 N. This results in an error of only 2.6% after 400,000 cycles.

Moreover the agreement with the semi-analytical calculation is very good. The values of the parameters of the damage law remain nearly the same. The similarity of results can be proved even better when plotting the stress distribution at the clamped cross-section during fatigue life (Figure 23). The values of the stresses are evaluated at numbers of cycles N, that are close to the values used in Figure 11 (due to the *cycle jump* approach, the values of the stresses are not available for each loading cycle from the finite element calculation). Of course, due to the fact that more than one element is used through the thickness and the Bernoulli assumption is no longer imposed, the stress distribution at cycle N = 1 is no longer linear, although no damage is present at that time. For the finite element analysis of each simulated loading cycle (stage 1 in Figure 20), the stress-strain relation in each Gauss-point is assumed to be linear and the Young's modulus is $E_0(1\text{-}D)$, where E_0 is the undamaged Young's modulus.

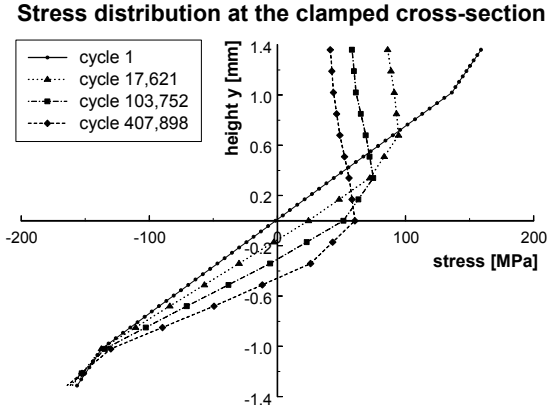

Figure 23 Distribution of the normal stresses at the clamped cross-section from finite element results.

Finally, Figures 23 and 24 show the growth of damage starting from the upper surface, subjected to the highest tensile stresses, and moving towards the neutral fibre of the laminate. The abscissa coincides with the length axis of the specimen (54.0 mm), while the ordinate axis represents the thickness of the specimen (2.72 mm), so that the plot area covers the complete cross-section of the free specimen length, as schematically indicated by the diagonal dashed lines. The damage distribution is shown for all elements, and the contours show lines of equal damage. Again damage is lying between zero (no damage) and one (complete failure).

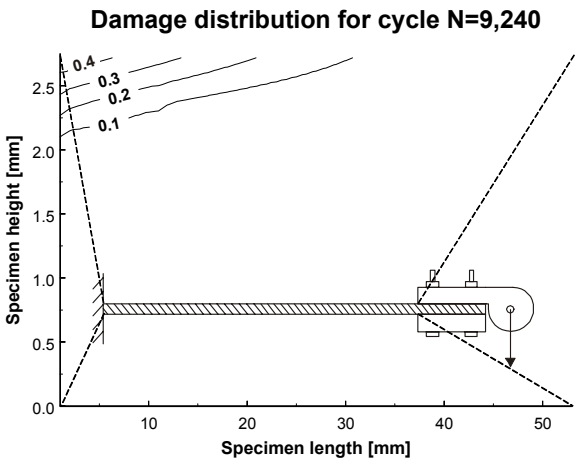

Figure 24 Damage distribution for N=9420

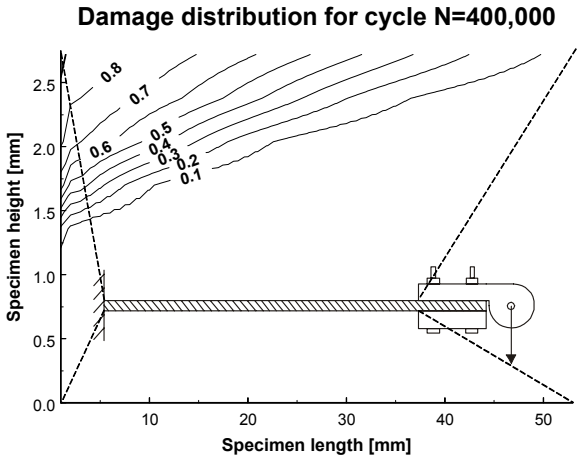

Figure 25 Damage distribution for N=208,763

Conclusions

Bending fatigue experiments were performed on plain woven glass/epoxy specimens with a $[\#45^{o}]_8$ stacking sequence. The observed stiffness degradation was modelled by using a local damage model with one scalar damage variable D.

First the fatigue damage model was implemented in a mathematical software package. It was shown that the damage curves are more reliable for extrapolation than the stress curves, because due to the stress redistribution during fatigue life, the stress components can increase or decrease without any foreknowledge.

Next the model was incorporated in a commercial finite element code, in such way that it is able to deal with two conflicting demands: (i) the continuous stress redistribution requires the simulation to follow the complete path of damage states, and (ii) finite element simulations should be fast and efficient in order to save time at the design stage of a composite component.

Using the *cycle jump* approach, the finite element implementation succeeds to meet both the demands. Each Gauss-point of the finite element mesh has been assigned an additional property: the value of the local *cycle jump*, inherent to each integration point of the mesh. The global *cycle jump* for the whole finite element mesh is defined as a percentile of the cumulative relative frequency distribution of all local *cycle jump* values.

The agreement with the experimental results was more than satisfying. Both the semi-analytical and the finite element implementation prove to be capable of modelling the stress redistribution across the structure and the stiffness degradation.

Acknowledgements

The author W. Van Paepegem gratefully acknowledges his finance through a grant of the Fund for Scientific Research – Flanders (F.W.O.), and the advice and technical support of Dr. Albert-Paul Gonze at the SAMTECH company. The authors also express their gratitude to Syncoglas for their support and technical collaboration.

References

[1] Carmet, A., Weber, B. and Robert, J.L. (2000). Fatigue Life Assessment of Components and Structures Under Multiaxial Service Loading. In : Bache, M.R. et al. (eds.). Fatigue 2000 : Fatigue & Durability assessment of materials, components and structures. Proceedings. Cambridge, 10-12 April 2000, Chameleon Press Ltd., pp. 295-304.

[2] Degrieck, J. and Van Paepegem, W. (2001). Fatigue Damage Modelling of Fibre-Reinforced Composite Materials: Review. Accepted for publication in Applied Mechanics Review.

[3] Van Paepegem, W. and Degrieck, J. (2000). Experimental setup for the bending fatigue of fibre-reinforced composite materials. In: Bache, M.R., Blackmore, P.A., Draper, J., Edwards, J.H., Roberts, P. and Yates, J.R. (eds.). Fatigue 2000 : Fatigue & Durability assessment of materials, components and structures. Proceedings. Cambridge, 10-12 April 2000, Chameleon Press Ltd., pp. 115-122.

[4] Van Paepegem, W. and Degrieck, J. (2001). Experimental setup for and numerical modelling of bending fatigue experiments on plain woven glass/epoxy composites. Composite Structures, 51(1), 1-8.

[5] Fujii, T., Amijima, S. and Okubo, K. (1993). Microscopic fatigue processes in a plain-weave glass-fibre composite. Composites Science and Technology, 49, 327-333.

[6] Schulte, K., Reese, E. and Chou, T.-W. (1987). Fatigue behaviour and damage development in woven fabric and hybrid fabric composites. In : Matthews, F.L., Buskell, N.C.R., Hodgkinson, J.M. and Morton, J. (eds.). Sixth International Conference on Composite Materials (ICCM-VI) & Second European Conference on Composite Materials (ECCM-II) : Volume 4. Proceedings, 20-24 July 1987, London, UK, Elsevier, pp. 4.89-4.99.

[7] Hansen, U. (1997). Damage development in woven fabric composites during tension-tension fatigue. In : Andersen, S.I., Brøndsted, P., Lilholt, H., Lystrup, Aa., Rheinländer, J.T., Sørensen, B.F. and Toftegaard, H. (eds.). Polymeric Composites - Expanding the Limits. Proceedings of the 18th Risø International Symposium on Materials Science, 1-5 September 1997, Roskilde, Denmark, Risø International Laboratory, pp. 345-351.

[8] Ferry, L., Gabory, D., Sicot, N., Berard, J.Y., Perreux, D. and Varchon, D. (1997). Experimental study of glass-epoxy composite bars loaded in combined bending and torsion loads. Fatigue and characterisation of the damage growth. In : Degallaix, S., Bathias, C. and Fougères, R. (eds.). International Conference on fatigue of composites. Proceedings, 3-5 June 1997, Paris, France, La Société Française de Métallurgie et de Matériaux, pp. 266-273.

[9] Herrington, P.D. and Doucet, A.B. (1992). Progression of bending fatigue damage around a discontinuity in glass/epoxy composites. Journal of Composite Materials, 26(14), 2045-2059.

[10] Chen, A.S. and Matthews, F.L. (1993). Biaxial flexural fatigue of composite plates. In : Miravete, A. (ed.). ICCM/9 Composites : properties and applications. Volume VI. Proceedings of the Ninth International Conference on Composite Materials, 12-16 July 1993, Madrid, Spain, Woodhead Publishing Limited, pp. 899-906.

[11] Sidoroff, F. and Subagio, B. (1987). Fatigue damage modelling of composite materials from bending tests. In : Matthews, F.L., Buskell, N.C.R., Hodgkinson, J.M. and Morton, J. (eds.). Sixth International Conference on Composite Materials (ICCM-VI) & Second European Conference on Composite Materials (ECCM-II) : Volume 4. Proceedings, 20-24 July 1987, London, UK, Elsevier, pp. 4.32-4.39.